15th World Congress on Computational Mechanics (WCCM-XV)
8th Asian Pacific Congress on Computational Mechanics (APCOM-VIII)
Virtual Congress: 31 July – 5 August 2022
S. Koshizuka (Ed.)

AVALANCHING OF VARIOUSLY SHAPED DEM PARTICLES

Dominik Krengel[1], Hans-Georg Matuttis[2] AND Mamoru Kikumoto[3]

[1] University of Tsukuba
1-1-1, Tennodai, Tsukuba, 305-8573, Japan
krengel.dominik.kb@u.tsukuba.ac.jp

[2] The University of Electro-Communications
1-5-1 Chofugaoka, Chofu, 182-8585, Japan
hg@mce.uec.ac.jp

[3] Yokohama National University
Tokiwadai 79-5, Hodogaya, Yokohama, 240-8501, Japan
kikumoto-mamoru-fc@ynu.ac.jp

Key words: Granular Materials, DEM, Shape Effects, Avalanching, Rotating Drum

Abstract. *Grains in most technically relevant granular materials are non-convex, while in discrete-element-simulations, convex particle shapes dominate. While differences in the physical behavior can be expected, the actual observables where these effects manifest are far from clear. In this research, we investigate how in a rotating two-dimensional drum, the physical behavior for rounded, irregular convex as well as non-convex shapes differs.*

1 Introduction

Rotating drums are one of the most commonly used setups to study dynamic equilibria of granular materials, as properties like angles of repose and stability as well as the release and halting of avalanches, can be investigated and compared over a wide range of different granular materials [2, 3, 6, 22]. Avalanches may be continuous or discrete, depending on the rotation speed of the drum [24] as well as the particle shape [5]. Beyond dynamic properties, particles with heterogeneous size dispersions may, due to their individual characteristics segregate [1, 4] or mix [1, 7], or give rise to pattern formation [9, 26].

Simulations of granular materials are performed either with discrete-element-methods (DEM) or continuum methods. While the DEM approach is much more limited in terms of system size and simulation time than the continuum approach, it allows to treat particles individually and to take into account the particle shape. Though realistic soil particles have complex, non-spherical shapes (see e.g. [23, 20] for classifications of sand grain shape), the majority of DEM-simulations are based on spheres or discs. More complicated particle shapes have been used, such as clusters of discs [12, 18], ellipsoids [11, 25] or, more recently, spheropolygons [11, 15] and their respective 3D-equivalents. Nevertheless, for hard-particle soft-contact simulations, the most controllable overlap computations are still performed via polygonal and polyhedral shapes (see [16] and references therein, because no intersection of curves must be computed. On the other hand, additional geometrical complexity can always be implemented for polygons and polyhedra by adding vertices. Unfortunately, studies utilizing convex polygonal particles in rotating drums remain scarce at best [10, 21], and studies with non-convex polygonal particles do not appear to exist at all (for non-convex polygons in bi-axial loading see [17]).

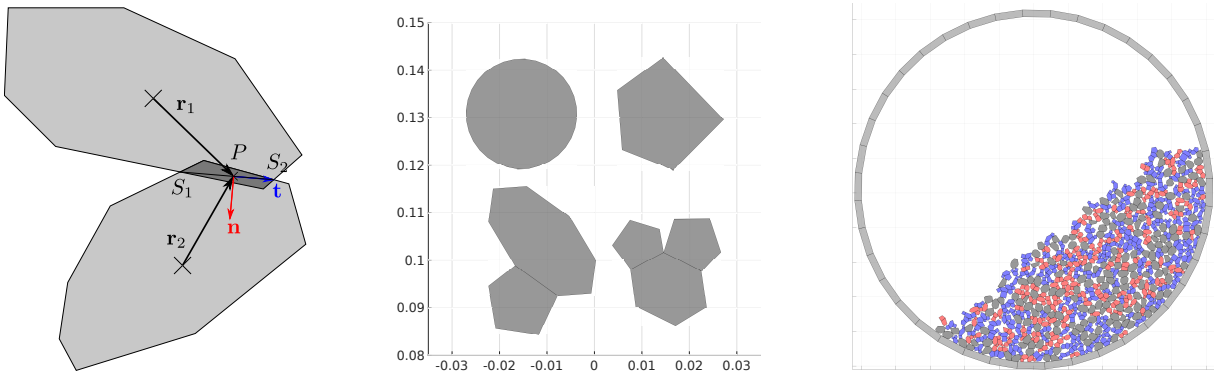

Figure 1: *Left*: Contact geometry for polygonal particles. The vectors $\mathbf{r}_1$ and $\mathbf{r}_1$ connect the particle center-of-masses and the centroid P of the overlap area (dark shading). The normal ($\mathbf{n}$) and tangential ($\mathbf{t}$) direction of the contact are given by the intersection points S_1 and S_2 of the overlap.
Center: Examples of round, convex and non-convex particles, the latter with two or three monomers. *Right*:Example of the filled drum during rotation. Particles with a single monomer are colored in gray, particles with two monomers are colored in red, and particles with three monomers are colored in blue.

As mentioned above, realistic granular materials are usually non-convex. It is therefore important to understand which observables of the granular bulk are affected when convex particles are replaced with non-convex particles. The aim of this work is to establish which differences in the dynamics of aggregates of round particles, convex polygonal particles and mixtures of convex and non-convex polygonal particles in a rotating drum exist, and which behavior is universal, or at least, common over a broad range of shapes. The granular dynamics in drums is restrained by quasi two-dimensional symmetry in axial direction, so the result in two dimensions should not totally be unlike those for three-dimensional simulations. In this article, we want to focus on the macroscopic differences in the behavior of avalanches due to the different shape of grains, which become most obvious at low rotation speeds of the drum. Our approach is therefore different from the one of Preud'homme et al.[19], who investigated avalanching at fast rotation speeds where differences between continuous vs. discrete avalanching get blurred.

2 Model description and sample preparation

2.1 Polygonal DEM

To model shape-dependent particle behavior in a rotating drum, we use a two-dimensional polygonal discrete element model (DEM) [16]. Figure 1, left) shows the geometry of two polygonal particles in contact. The tangential direction ($\mathbf{t}$) is obtained from the connecting line between the intersection points (S_1, S_2). Consequently, the normal direction ($\mathbf{n}$) is also fixed. The elastic force is taken as a function of the overlap area A as measure of the deformation of the particles and the Young's modulus Y as

$$F_{\mathrm{el}} = \frac{YA}{l}, \tag{1}$$

with the characteristic length $l = 4\dfrac{\mathbf{r}_1\mathbf{r}_2}{\mathbf{r}_1+\mathbf{r}_2}$ for contact vectors $\mathbf{r}_1$, $\mathbf{r}_2$. Normal dissipation is modeled in analogy to the linear oscillator as

$$F_{\mathrm{diss}} = \gamma\sqrt{mY}\frac{\dot{A}}{l}, \tag{2}$$

Table 1: Material and simulation parameters.

Num. of particles	N	492	Material density	ρ	$5000\,[\mathrm{kg/m^2}]$
Friction coefficient	μ	0.5	Young's modulus	$Y_{2D} = Y$	$10^9\,[\mathrm{N/m}]$
Average particle radius	$\overline{R}$	$1.225 \cdot 10^{-2}\,[\mathrm{m}]$	Drum diameter	R_{drum}	$0.5\,[\mathrm{m}]$
Drum velocity	ω	$\frac{\pi}{20}, \frac{\pi}{30}, \frac{\pi}{50}, \frac{\pi}{70}\,[\mathrm{rad/s}]$	Timestep	dt	$1 \cdot 10^{-5}\,[1/s]$

with the reduced mass m of the contacting particles and damping constant γ. To avoid reversing the elastic force through overcompensation due to the damping force in equation 2, a cutoff is required so that the normal force will not become attractive. Solid friction is implemented in tangential direction in a DAE formulation [13]. Residual noise in the static friction force does not affect the dynamics of the particles in a rotating drum. The torques are computed from the sum of the normal and tangential forces $\mathbf{F}$ and the contact vectors $\mathbf{r}_{1,2}$ as $\mathbf{T}_{1,2} = \mathbf{r}_{1,2} \times \mathbf{F}$.

Table 1 shows the used material parameters. While the Young's modulus may look small, it should be noted that it affects only the force computation, where in real particles, rough surfaces are in contact, so that the effective material strength at the surface is also considerably reduced compared to the material's bulk Young's modulus. The particles themselves (i.e. their outlines) are rigid.

2.2 Sample preparation

In this research we consider three different assemblies: a mixture of irregular-convex (i.e. convex polygons which are not equiangular) and non-convex polygons, an assembly of only convex polygons, and an assembly of round particles. Irregular convex particles are created by randomly distributing points P_i on the perimeter of a circle with radius $\overline{R}$ with a minimum internal angle for each corner. The circle then is stretched into an ellipse with the long axis being up to 1.5 times longer than the short axis, and the points P_i are taken as the corners of the irregular convex polygon. The stretching factor between 1 and 1.5 is selected from equally distributed random numbers. Non-convex particles are created as rigid clusters of two or three convex particles, rigidly connected along their contacting edges, with the circumradius of the whole cluster being approximately $\overline{R}$. The median particle area is $A_{\mathrm{med}} = 3.72 \cdot 10^{-2}$ m^2. Figure 2, left) shows the distribution of particle areas within the assembly. To generate the assembly of only convex particles we replace the non-convex particles with their convex hull and downscale the newly generated convex particles to match the area of the original non-convex particles. The convex particles remain unchanged. As we preserve the particle number and the distribution of particle sizes with this method, this ensures that our simulations with differently shaped particles are as comparable as possible. Likewise, to generate configurations of round particles we replace all particles with regular convex polygons (with 32 corners) of the same area. We use regular convex polygons with 32 corners instead of round particles, as they have nearly the same tendency to roll, so the difference to the dynamics of ideal circular particles should be negligible. Figure 1, center) shows typical particle shapes and -dimensions. To generate the simulation set-up, a random mixture of convex and non-convex particles is initialized inside a drum which consists of an annulus composed of 40 isosceles trapezoids, see figure 1, right). The mixture consists of 178 convex particles and 314 non-convex particles, with the non-convex particles making up 62% of the bulk area. The area distribution of convex and non-convex particles within the mixture is shown in figure 2, right). In the case of only convex or round particles, the particles are replaced with their respective new shapes as described above. The particles drop under gravity and settle for three seconds before the drum begins to rotate. All configurations are run for 5 full drum

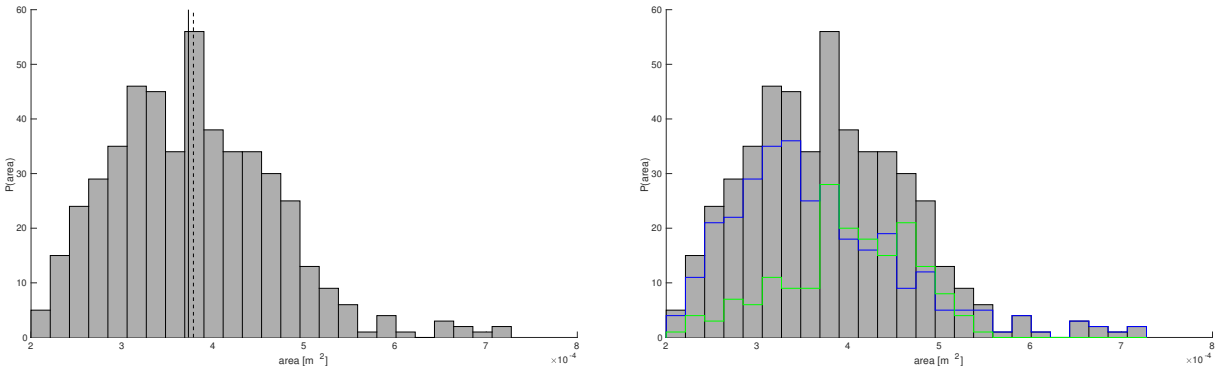

Figure 2: *Left*: Distribution of the particle areas A in the aggregates. The solid black line marks the median area of the particles, the dashed line marks the mean area. As the area of each individual particle is the same in all configurations, this distribution is valid for all simulations.
Right: Area distribution of the non-convex particles (blue) and convex particles (green) within the convex–non-convex particles mixture (gray).

rotations, regardless of the drum's angular velocity.Discrete avalanches are produced by rotating the drum at four different angular velocities between $\omega = \frac{\pi}{20}\,[\mathrm{rad/s}]$ and $\omega = \frac{\pi}{70}\,[\mathrm{rad/s}]$, the regime of angular velocities below the occurrence of continuous avalanches also for the round particles. The drum is rotating slow enough so that discrete avalanches also occur for round particles.

3 Results and discussion

3.1 Critical angle

To equilibrate the particle packing, we rotate the drum for 60 seconds with an angular velocity of $\omega = \frac{\pi}{30}$ for all configurations. Afterward, the drum filling is left to relax for 3.5 seconds. Then we perform five additional stop-and-go cycles by slowly accelerating the drum to $\omega = \frac{\pi}{30}$, keep it at this speed for 3.5 seconds, and slowly decelerate it until it stops and let it rest for 3 seconds. We compute

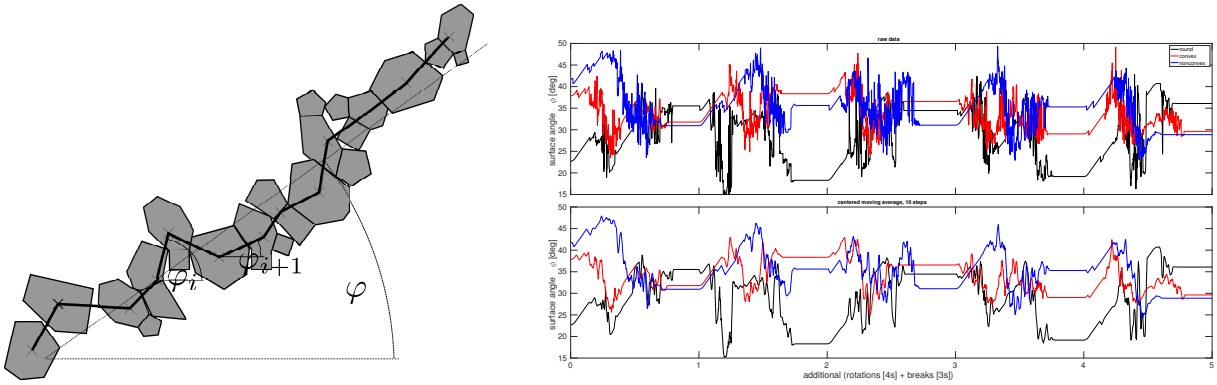

Figure 3: *Left*: The local slope is given by the traverse (bold line) through the centroids of the particle near the free surface of the alpha-shape, with the average inclination φ as the direct average of the local inclination φ_i. *Right*: Evolution of the surface angle for different particles shapes in a drum rotating with $\omega = \frac{\pi}{30}$. Top: raw data, bottom: 10-step moving average.

the alpha-shape [8] (simply speaking, the generalization of the convex hull for non-convex shapes with a length-cutoff alpha) of all particles with an alpha radius of three times the average particle radius. From the particles which are located near the free surface of the alpha-shape we fit the angles of the local slopes, φ_i along the traverse through the centroids of the particles (figure 3, left)). The surface angle of the aggregate is averaged over all these angles, $\varphi = \frac{1}{N}\sum_{i=1}^{N}\varphi_i$, see Baumann et al. [3] for similar use of the local slope. For large numbers of particles this method would reduce to the conventional method of fitting a straight line through the centroids of all particles on the free surface and measuring its slope.

For a granular aggregate created by avalanches, the slope is given by the finite angle of repose, φ_R. The slope will be stable under tilting up to the angle of marginal stability, φ_{MS}, when avalanches appear and the inclination decreases [14].

We plot the time evolution of the surface angle for assemblies of round particles, convex particles and non-convex particles in figure 3, right). While the drum is at a standstill, the average angle of repose for round particles is around $\varphi_R = 18.7°$, significantly lower than for non-round particles. For convex particles, the lowest angle of repose is found to be $\varphi_R = 29.3°$, while for non-convex particles the angle of repose is at $\varphi_R = 28.8°$, almost identical to the angle for convex particles. The angle of marginal stability is $\varphi_{MS} = 38.42 \pm 1.49°$ for round particles, $\varphi_{MS} = 41.38 \pm 1.9°$ for convex particles and $\varphi_{MS} = 45.14 \pm 2.26°$ for non-convex particles. That means, under equivalent conditions, avalanches in configurations of non-convex particles are triggered later than in configurations of convex particles, while the avalanches come to rest at nearly identical angles of repose. That an actual angle of repose for non-convex particles is smaller than for convex particles is a statistical fluctuation.

3.2 Bulk center-of-mass behavior

One of the tenets of nonlinear mechanics is that differences in the dynamics should become obvious in the dynamical system, i.e. when plotting a suitable set of coordinates versus a suitable set of velocities.

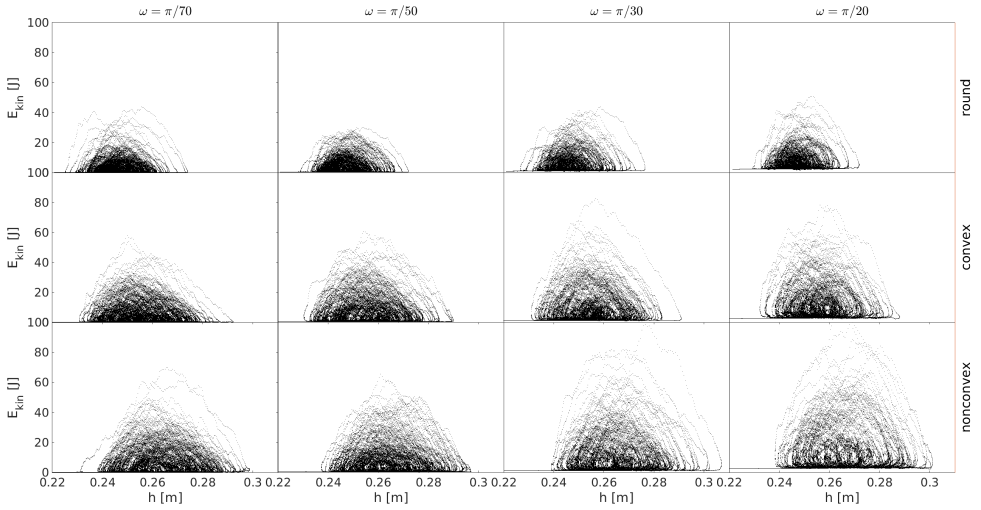

Figure 4: Translational kinetic energy of the bulk over the center-of-mass height during five full rotations of the drum (The horizontal line at the bottom left of each cycle marks the trajectory of the center-of-mass, and as an initialization effect, is negligible).

For complex systems (continua or many-body systems), suitable averages instead of the elementary variables can be used. In our investigation, we have used the average kinetic energy instead of the average velocity to eliminate the velocity direction.

In figure 4 we plot the bulk translational kinetic energy against the bulk center-of-mass height for the whole of five rotations, and obtain cycles of varying width and height. The data is plotted from the onset of drum rotation on, thus there is a negligible, non-zero offset depending on the angular velocity of the drum. For aggregates of round particles (first row in figure 4), we find that the cycles are significantly more compact than for convex or convex–non-convex mixtures (second and third row in figure 4). As the rotation speed of the drum increases, the cycles fray out and expand along the energy axis. With an increase of the rotation speed, the cycles stray away from few discrete paths to a more continuous variation, while the total range of energy and height variation is not affected. Some single cycles can nevertheless be larger than the majority of the trajectory distribution due to statistical fluctuations. The influence of the particle shape on the cycles is obvious in the variation of the center-of-mass (wider extension along the horizontal axis, with a shift to the right), as well as an increase in the variation of the energy. This indicates on average larger height differences and a larger variation in the size and speed of the avalanches.

A similar tendency is observed in the rotational energy, see figure 5. (We plot the rotational energy of the particles relative to the rigid-body rotation of the drum, therefore we have an initial tail with $E_{\mathrm{rot}} = 0$ [J] before the onset of the first avalanche on the left side of the structures.) At low rotation speeds, the cycles follow some discrete paths. At high rotation speeds, however, the center-of-mass of round particles follows more compact paths, while for convex, and especially non-convex particles, the center-of-mass paths fray out. In addition, non-round particles show an increase in the variation of the energy, especially in the left half of the structures, while round particles do not show any such increase. In particular non-convex particles are more likely to roll (compared to convex particles), as due to their shapes their centers-of-mass are supported at several points, and therefore, less stable. No configuration shows a

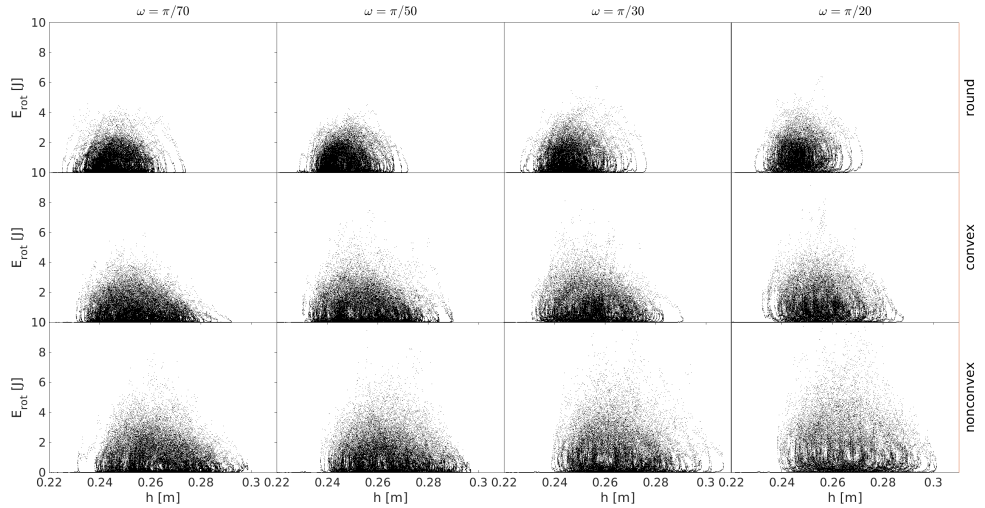

Figure 5: Rotational energy of the bulk with respect to the center-of-mass height during five full rotations of the drum. The horizontal line at the bottom marks the center-of-mass location from the onset of rotation to the onset of avalanching.

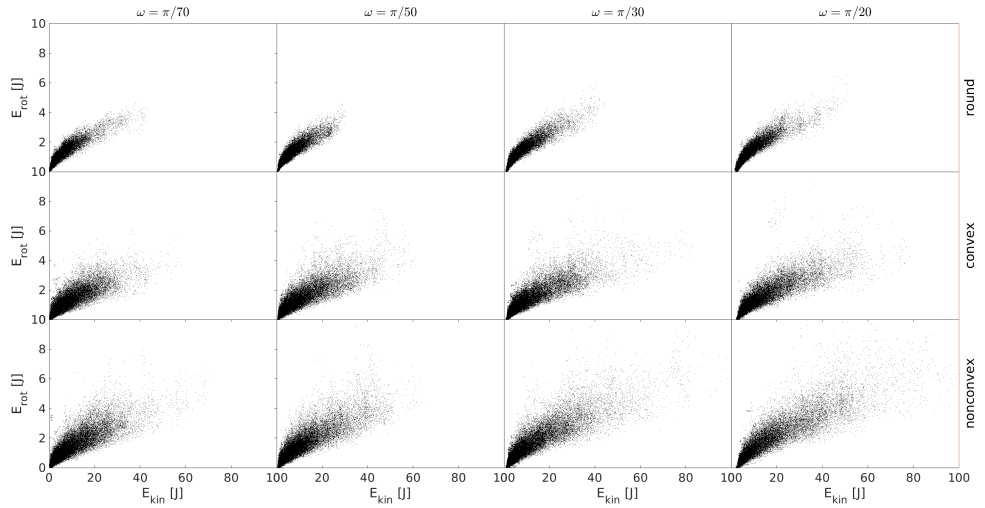

Figure 6: Translational and rotational rotational energy during five full rotations of the drum.

strong increase in their extension along the horizontal axis with increasing drum rotation. However, the cycles extend further to the right with increasing complex particle shape, indicating steeper slopes on the surfaces (compare section 3.1 for the surface angle).

Plotting the translational against the rotational kinetic energy (see figure 6) we see a change towards higher energies in both axes with increasingly complex particle shapes (i.e. from "round" to convex to non-convex). Differences between convex and non-convex particles become more apparent as the angular velocity of the drum increases, while on the other hand, for round particles the distribution of the kinetic energy of the rotation remains largely unaffected by the rotation speed of the drum.

3.3 Identification of avalanches

Determining avalanches in systems like those inside drums is not easy: The movement of the center-of-mass may be due to one large avalanches or two smaller independent ones. Even a small avalanche on top of a larger one (each with different velocity) is conceivable. For tractability, we define an avalanche as the set of all particles whose velocity relative to the drum was above the threshold velocity of $v_{\text{thresh}} = 0.05$ [m/s]. For lower velocity thresholds, avalanches are not reliably detected, while for higher thresholds, particles which are moving due to relaxation of the granular matrix but are otherwise not part of the avalanche and are erroneously identified. Additionally, filtering the with respect to the direction of their movement relative to the drum has very little influence on statistics of the avalanches. The center-of-mass of the granular filling of the drum and its translational kinetic and rotational energy are recorded every 500 timesteps (i.e. every 0.005 seconds). The full physical information of the system, i.e. particle center-of-mass location, velocity and angular velocity, acceleration, as well as the location of the corners was recorded every 1000 timesteps (every 0.01 seconds).

3.4 Onset and motion of avalanches for non-convex particles

Next, we discuss the behavior of avalanches for non-convex particles, along the sequence of selected screenshots in figure 7. Avalanches in mixtures of convex and non-convex particles tend to start in the

upper half of the slope as in figure 7,a)-b), where the "forward-momentum" is largest, though usually not on the top, because friction with the wall is largest. While the avalanche is slowly taking up speed, the surface profile tends to bulge out so that the initial straight surface starts to bulge out in the upper third of the slope as in figure 7,c). Simultaneously, in the interface between the avalanche (red particles) and the non-avalanching bulk (gray particles), the inter-particle contacts get loosened and a shear zone forms. Once the bump in the top collapses due to particles below sliding away, the speed of the avalanche increases and some particles may become airborne, as in figure 7,d)-g). Eventually the avalanche slows down as particles are stopped by the wall of the drum or in gaps in the interface as in figure 7,h). The region of avalanching particles migrates towards the upper half of the slope as in figure 7,i), until finally, as in figure 7,j) all particles become immobile again.

3.5 Avalanche properties

In figure 8 we plot the velocity of the avalanche v against the center-of-mass height h of the avalanche at each timestep. For round particles, the data points are concentrated in a bell-like shape, with the highest velocities measured in the center of the slope, i.e. the middle of the distribution. As the rotation speed of the drum increases, the data points start to concentrate in a ball-like structure in the center of the slope. Compared to the other particle configurations, round particles show higher velocities at the low end of the slope, as can be seen in an additional structure on the left side of the graph. Particles in contact with the drum may act like ball bearings upon which the bulk can slide down without avalanching until the free surface is almost horizontal again. This effect is only possible for two-dimensional simulations, as in three-dimensional simulations, or quasi two-dimensional experiments with rod-like particles, frictional contacts with the side walls would provide additional stabilization. The velocity-distribution for aggregates of convex and non-convex particles likewise resembles a bell-shape at low drum rotation velocities ($\omega = \pi/70$ [rad/s] and $\omega = \pi/50$ [rad/s]). However, the velocity distribution on the bottom end of the slope (on the left side of the diagrams) is notably lower than the distribution on the right side of the diagrams. As the drum velocity increases, the left part of the distributions reduces until it almost vanishes

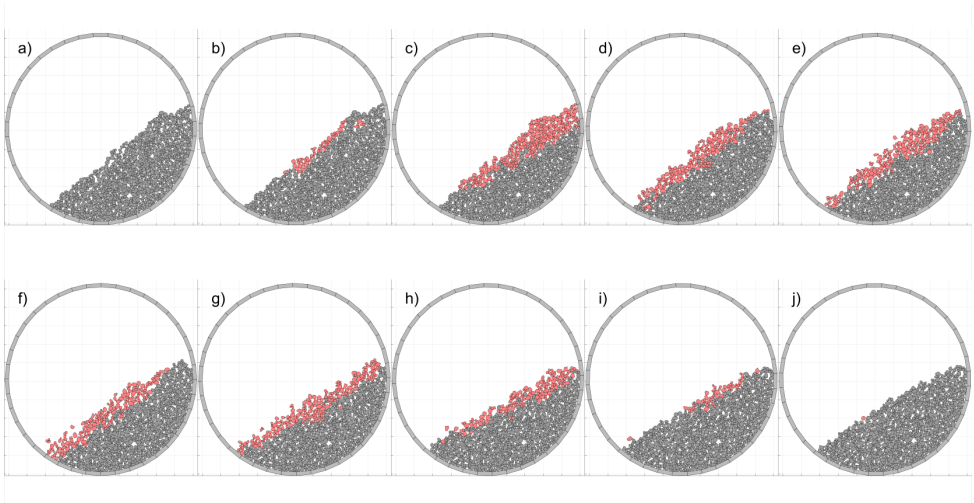

Figure 7: Time sequence of an avalanche with non-convex particles in a drum rotating with $\omega = \frac{\pi}{50}$. Mobile particles above threshold velocity are highlighted in red to emphasize the avalanche.

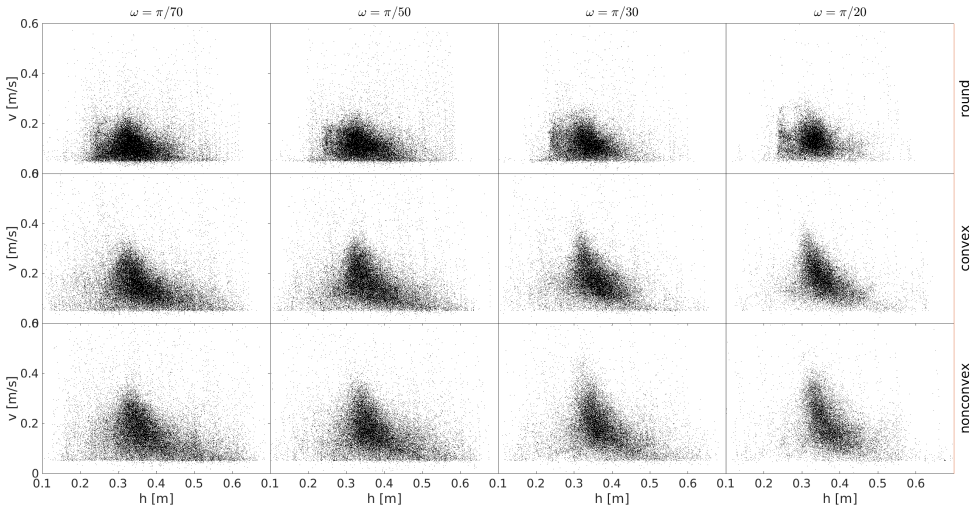

Figure 8: Velocity of the center-of-mass of the avalanches with respect to their respective center-of-mass height.

at $\omega = \pi/20$ [rad/s]. In a similar manner, the right side of the distribution becomes smaller, although not as notably. On the other hand, the velocity distribution is stronger in the center of the slope, between 0.3 and 0.4m for systems of convex particles and of non-convex particles than for the equivalent systems of round particles. In summary, while the velocity-distributions show differences between systems of round particles and systems of non-round particles, they can not be used to differentiate between convex and non-convex particles.

As particle shape influences packing density of granular aggregates, one might suspect that it influences the density of granular avalanches as well. We therefor determine the area of the avalanches by computing the alpha-shape over all particles identified as belonging to the avalanche, as described in section 3.3. The density of the avalanche, ρ, is then determined by dividing the sum of the area of all par-

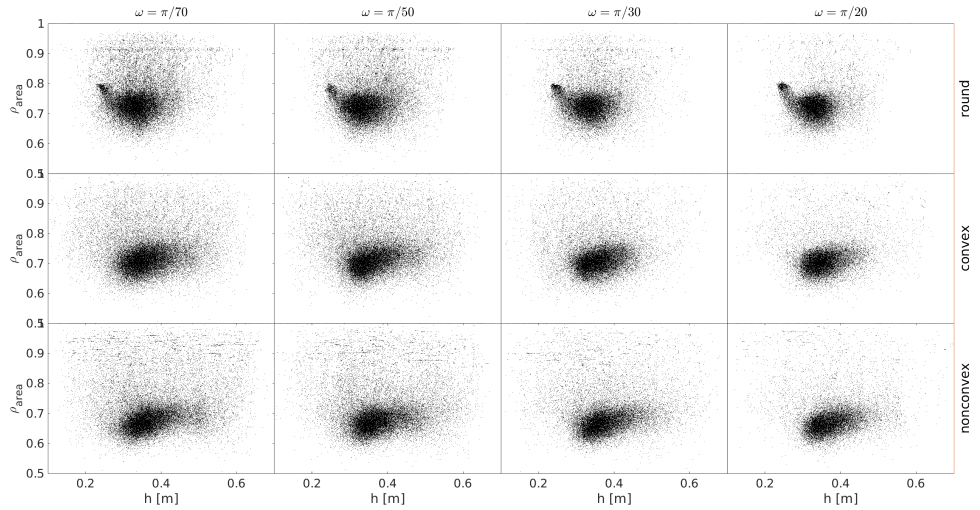

Figure 9: Density of the avalanches with respect to the area of their convex hull.

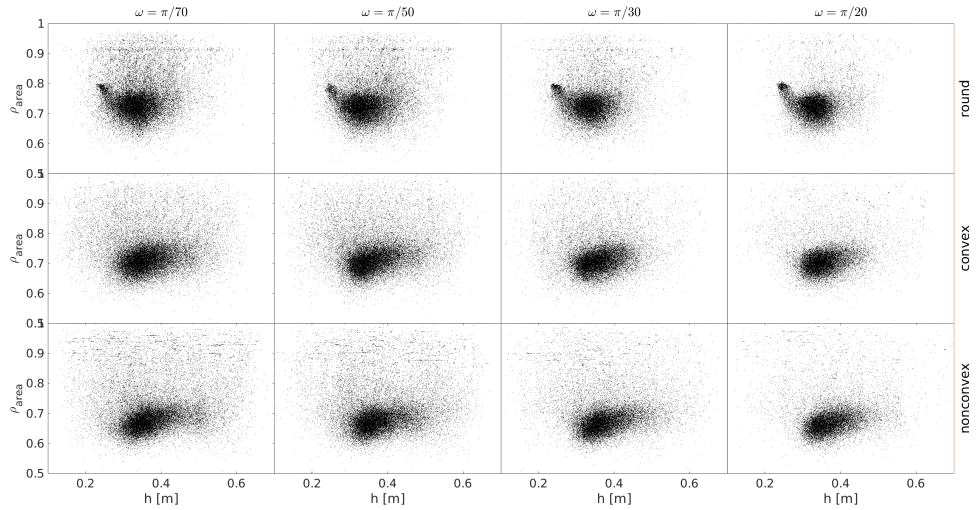

Figure 10: Number of particles moving in the avalanche relative to the total number of particles in the drum.

ticles within the avalanche by the area of the avalanche. We plot the resulting distribution of avalanche density over the center-of-mass height of the avalanche in figure 9. For all of the different configurations we obtain an oval distribution in the middle of the diagram. For configurations of round particles we obtain an additional high-density structure on the left side of the diagram due to sliding of the entire aggregate, replicating the results from the velocity distributions. On the other hand, the distributions for convex and non-convex particles show a concentration of velocities on the right side of the diagram, in higher parts of the slope. For non-convex particle assemblies, the distributions stretch further to the right than for convex particle assemblies. Besides, avalanches of non-convex particles appear to slightly lower density than avalanches of convex particles for equal velocities of the drum (rows two and three in figure 9, in particular at $\omega = \pi/30$). In general, the diagrams in figure 9 for non-round particles show a wider scattering along the *h*-axis than the diagrams for round particles, in particular at higher values of ρ. While the distributions in general become more concentrated for higher drum velocities for any of the configurations, for non-convex particle assemblies the scattering decreases the least.

To determine the ratio $N/N_{\max}$ of particles mobilized during the progress of the avalanche we can simply count the number of particles N that have been identified as belonging to an avalanche see section 3.3. In figure 10 we plot the distribution of mobilized particles with respect to their center-of-mass height. For round particles, we again see the entire aggregate sliding down the drum, expressed in a long "neck" of the distribution sloped to the left. The bulk slides independently of the angular velocity of the drum. In aggregates of convex particles and mixtures of convex- and non-convex particles similar amounts of particles are mobilized over the whole live span of the avalanche. Most particles are mobilized when the avalanche is in the center of the slope, i.e. at the middle of the horizontal axis. Avalanches that reach the bottom of the slope contain lower number of particles, as more particles are deposited in the slope bed higher on the slope. As the drum velocity increases, the distribution becomes less dense at lower values of $N/N_{\max}$, i.e. larger avalanches become more likely. In general, while avalanche properties allow to differentiate well between avalanches of round particles and avalanches of non-round particles, they are less suitable to distinguish between avalanches of convex particles and avalanches of non-convex particles.

4 Conclusion

We have carried out simulations of rotating drums using a polygonal Discrete-Element-Method in order to explicitly describe the difference in the dynamics between aggregates of round, convex polygonal and non-convex polygonal particles.

We find that aggregates of round particles are clearly distinguished from aggregates of non-round particles, whether convex or non-convex, in a parameter space describing the whole of the aggregate, as well as in the behavior of avalanches, due to the differences in particle mobility and strength of solid friction. On the other hand, the deviations in the behavior between aggregates of irregular convex and non-convex particles are less marked. We find differences in the angle of marginal stability, as avalanching starts at a higher slope angle for non-convex particle aggregates compared to aggregates of convex particles, but both mixtures revert to the same steady-state angle after an avalanche. We see further differences between convex and non-convex particles in the distribution of the phasespace trajectories of the bulk center-of-mass, where the cycles for the translational energy of the height and the rotational energy of the height are more compact for convex particles than for non-convex particles, while these differences are less pronounced for round particles. On the other hand, the differences in the dynamics of avalanches are less suitable to differentiate between convex and non-convex particles. Avalanches of both convex and of non-convex particles mobilize similar amounts of particles though the avalanches of non-convex particles tend to have lower density than avalanches of convex particles. At the same time, both mixtures show similar height-velocity profiles at any of the investigated angular velocities of the drum, rendering the avalanche velocity unsuitable to discriminate between the mixtures. While the parameters discussed in section 3 all to some degree allow to discriminate between aggregates of convex and of non-convex particles, other parameters are meaningless: Avalanches in non-convex aggregates follow the same acceleration profile as they do in aggregates of convex particles. Likewise, the acceleration of the bulk shows the same structures for either of the non-round particles. Also, time-series of the translational and rotational kinetic energy for convex-particles are indistinguishable from those for non-convex particles. And finally, velocity distributions in avalanches and the evolution of these distributions are the same for convex and non-convex particles.

REFERENCES

[1] Arntz, M. M. H. D. and den Otter, W. K. and Briels, W. J. and Bussmann, P. J. T. and Beeftink, H. H. and Boom, R. M. Granular mixing and segregation in a horizontal rotating drum. *AIChE Journal* (2008) **54**:3133–3146.

[2] Balmforth, N. J. and McElwaine, J. N. From episodic avalanching to continuous flow in a granular drum. *Granular Matter* (2018) **52**:1–2.

[3] Baumann, G. and Janosi, I. M. and Wolf D. E. Surface properties and flow of granular material in a two-dimensional rotating-drum model. *Physical Review E* (1995) **51**.

[4] Cantelaube, F. and Bideau, D. and Roux, S. Kinetics of segregation of granular media in a two-dimensional rotating drum. *Powder Technology* (1997) **93**:1–11.

[5] Chen, J. and Krengel, D. and Matuttis, H.-G. Experimental study of particle shape dependence of avalanches inside a rotating drum. *EPJ Web of Conferences* (2021) **249**:06001.

[6] Chen, Q. and Yang, H. and Li, R. and Xiu, W. Z. and Han, R. and Sun, Q. C. and Zivkovic, V. Compaction and dilatancy of irregular particles avalanche flow in rotating drum operated in slumping regime. *Powder Technology* (2020) **364**:1039–1048.

[7] Clément, E. and Rajchenbach, J. and Duran, J. Mixing of a Granular Material in a Bidimensional Rotating Drum. *Europhysics Letters* (1995) **30**:7–12.

[8] Edelsbrunner, H. and Ernst P. Mücke, E. P. Three-Dimensional Alpha Shapes. *ACM Transactions on Graphics* (1994) **13**:43–72.

[9] Hill, K. M. and Caprihan, A. and Kakalios, J. Axial segregation of granular media rotated in a drum mixer: Pattern evolution. *Physical Review E* (1997) **56**:4386–4393.

[10] Höhner, D. and Wirtz, S. and Scherer V. A study on the influence of particle shape and shape approximation on particle mechanics in a rotating drum using the discrete element method. *Powder Technology* (2014) **253**:256–265.

[11] Kafashan, J. and Wiacek, J. and Rahman, N. A. and Gan, J. Two-dimensional particle shapes modelling for DEM simulations in engineering: A review. *Granular Matter* (2019) **21**.

[12] Khazeni, A. and Mansourpour, Z. Influence of non-spherical shape approximation on DEM simulation accuracy by multi-sphere method. *Powder Technology* (2018) **332**:265–278.

[13] Krengel, D. and Matuttis, H.-G. Implementation of Static Friction for Many-Body Problems in Two Dimensions. *Journal of the Physical Society of Japan* (2018) **87**:124402.

[14] Lee, J. and Herrmann, H. J. Angle of repose and angle of marginal stability: molecular dynamics of granular particles. *Journal of Physics A* (1993) **26**:373–383.

[15] Lu, G. and Third, J. R. and Müller, C.R. Discrete element models for non-spherical particle systems: From theoretical developments to applications. *Chemical Engineering Science* (2015) **127**:425–465

[16] Matuttis, H.-G. and Chen, J. *Understanding the Discrete Element Method*. Wiley, (2014).

[17] Matuttis, H.-G. and Nawa, M. and Krengel, D. Stress-Strain diagrams for non-convex particles. *EPJ Web of Conferences* (2017) **140**:06005.

[18] Norouzi, H. R. and Zarghami, R. and Mostoufi, N. Insights into the granular flow in rotating drums. *Chemical Engineering Research and Design* (2015) **102**:12–25.

[19] Preud´homme, N. and Opsomer, E. and Vandewalle, N. and Lumay, G.. Effect of grain shape on the dynamics of granular materials in 2D rotating drum. *EPJ Web of Conferences* (2021) **249**:06002.

[20] Powers, M. C. A New Roundness Scale for Sedimentary Particles. *SEPM Journal of Sedimentary Research* (1953) **23**.

[21] Rakotonirina, A. *Fluid-solid interaction in a non-convex granular media*. Université de Lyon, (2016).

[22] Ristow, G. H. Dynamics of granular materials in a rotating drum. *Europhysics Letters* (1996) **34**:263–268.

[23] Russell, R. D. and Taylor, R. E. Roundness and Shape of Mississippi River Sands. *The Journal of Geology* (1937) **45**:225–267.

[24] Santomaso, A. C. and Ding, Y. L. and Lickiss, J. R. and York, D. W. Investigation of the Granular Behaviour in a Rotating Drum Operated over a Wide Range of Rotational Speed. *Chemical Engineering Research and Design* (2015) **81**:936–945.

[25] Yang, S. and Sun, Y. and Chew, J. W. Simulation of the granular flow of cylindrical particles in the rotating drum. *AIChE Journal* (2018) **64**:3835–3848.

[26] Zuriguel, I. and Gray, J. M. N. T. and Peixinho, J. and Mullin, T. Pattern selection by a granular wave in a rotating drum. *Physical Review E* (2006) **73**.